

Potentiostatic-Potentiodynamic Reduction Synthesis of Anthraquinone Functionalized Graphene for Oxygen Reduction in Alkaline Medium

Guoquan Zhang^{*}, Yufei Zhou, Jie Chen, Fenglin Yang^{**}

Key Laboratory of Industrial Ecology and Environmental Engineering, Ministry of Education, School of Environmental Science and Technology, Dalian University of Technology, Dalian 116024, P.R. China

*E-mail: guoquanz@126.com

**E-mail: yangfl@dlut.edu.cn

Received: 23 August 2012 / Accepted: 28 September 2012 / Published: 1 November 2012

Through direct electrochemical potentiostatic-potentiodynamic reduction of the starting materials of graphene oxide (GO) and Fast Red Al Salt, the anthraquinone functionalized graphene nanocomposite was developed as a highly efficient electrocatalyst for oxygen reduction reaction (ORR) in alkaline conditions. Scanning electron microscopy, Transmission electron microscopy, X-ray diffraction, Raman and X-ray photoelectron spectroscopy characterizations revealed that the most of oxygen-containing functional groups on GO were removed after electroreduction. The electrocatalytic ORR have systematically investigated by cyclic voltammetry, rotating disk electrode and rotating ring-disk electrode techniques. Results show that the anthraquinone covalently functionalized graphene afforded much greater electrocatalytic activity towards ORR in 0.1 M KOH than the sole graphene and anthraquinone covalently bonded glass carbon materials. At anthraquinone/graphene modified electrode, two reduction processes both attributed to $2e^-$ reduction are recorded for ORR with HO_2^- as intermediate. The presence of graphene nanosheets not only results in larger peak current and shifts the onset potential of ORR in the positive direction, but also leads to further reduction of partial HO_2^- to OH^- in the more negative potential region.

Keywords: Anthraquinone; Electrocatalysis; Graphene; Nanocomposite; Oxygen reduction reaction

1. INTRODUCTION

In recent years, the increasing study has been focused on the oxygen reduction reaction (ORR) due to its significance in both theoretical and practical application, such as electrochemical energy conversion in fuel cells [1,2] and electrochemical advanced oxidation processes [3] in wastewater treatments. Generally, the ORR proceeds by a $2e^-$ pathway or via a direct $4e^-$ pathway or via two $2e^-$

pathway, depending on the electrode materials and its surface properties as well as the solution pH [4,5]. The kinetics of the ORR is usually very slow, and thus electrocatalyst design is a key factor for enhancing the performance of cathodes towards ORR.

Considering the practical importance of the electrogeneration of hydrogen peroxide, many mediators have been employed as electrocatalysts for the $2e^-$ reduction of oxygen to produce peroxide. Among them, quinones (phenanthrenequinone (PQ), naphthoquinone (NQ), anthraquinone (AQ)) [5–10] and their various derivatives have been regarded as the ideal metal-free electrocatalysts for ORR. It is generally considered that oxygen reduction on quinonoid compound modified carbon-based cathodes involves the formation of peroxide in alkaline and acidic media. However, adsorptive quinones tend to desorb from the electrode surface during the long-term operation, especially in alkaline solution ($\text{pH} > 10$) [11]. It is more beneficial to enhance the oxygen reduction rate and electrode stability via covalent attachment of the quinone moieties by electrochemically reducing the corresponding diazonium salts [6,8–10]. Moreover, it has been recently shown that the modification of electrode by the dispersion of electrocatalysts at molecule level throughout the well-defined matrix of conductive/electroactive support materials, such as conducting polymers and carbon nanotubes, provides higher specific surface, more active sites and higher stability.

Graphene, a two-dimensional sheet of sp^2 conjugated carbon atoms can be considered as giant polyaromatic platform for performing chemistry due to its open-ended structure. Because of its fascinating and extraordinary structure, high specific surface area and high electrical conductivity, graphene has created a new area of nanomaterial and nanotechnology science. Moreover, since the pioneering work regarding the low-cost and large-scale synthesis of graphene nanosheets through the electrochemical reduction method was published [12], graphene has been widely used as electrocatalyst support and grafted with many functional materials to form nanocomposites (e.g. Nitrogen-doped graphene) for various applications in many aspects of electrochemical technology [13–27].

To utilize the advantages of both graphene and anthraquinones, we have recently constructed anthraquinone/graphene nanocomposite modified electrodes and studied the ORR in neutral medium [28]. Taking into account of the well known fact that the higher electroactive properties of carbon materials for oxygen reduction achieved at higher pHs, due to the significant decrease in overpotential for the first electron transfer of dissolved oxygen in alkaline media [29], in this work the ORR was therefore carried out in 0.1 M KOH on the anthraquinone functionalized graphene nanosheets synthesized by the electrochemical potentiostatic-potentiodynamic reduction method using the cyclic voltammetry (CV), rotating disk electrode (RDE) and rotating ring-disk electrode (RRDE) techniques. The purpose of the present work was to determine the predominant pathway of the ORR and to further estimate the electrocatalytic contribution of AQ and graphene nanosheets to the overall ORR in the enlarged potential range with more negative cathodic limit.

2. EXPERIMENTAL

All chemicals were of analytical grade and used as received without further purification. Graphene oxide (GO) were synthesized from natural flake graphite (600 mesh, 99.9%) according to

the modified Hummer's method [30]. The as-synthesized GO was dispersed in distilled water and subjected to ultrasonication for 2 h, then centrifuged to remove any unexfoliated graphite oxide particles. Because of the existence of plentiful of polar oxygen-containing functional groups on the edges and planar surfaces of the individual GO sheets, a stable and well-dispersed GO aqueous suspension (0.5 mg mL^{-1}) with yellow-brown color was thus obtained (Fig.1(a)) with the aid of ultrasonication.

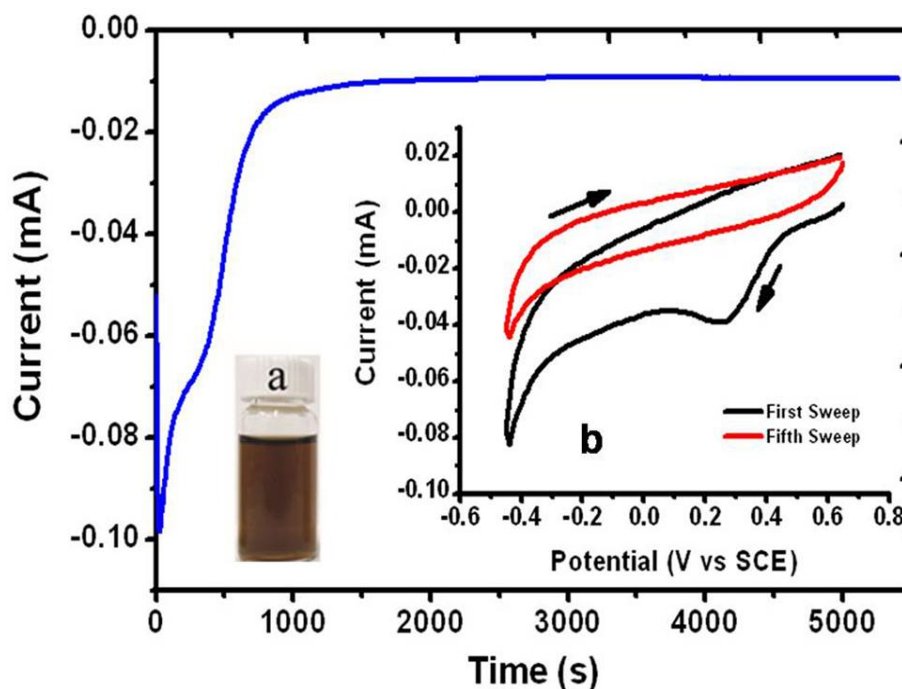


Figure 1. Typical current-time curve for the potentiostatic reduction of GO film on a GC electrode (5 mm diameter) with an applied potential of -1.0 V in N_2 -saturated 0.1 M PBS. The inset shows (a) Photograph image of the GO aqueous suspension (0.5 mg mL^{-1}), (b) First and fifth sweeps for the potentiodynamic grafting of AQ on ER-GO/GC in N_2 -saturated acetonitrile containing 10 mM Fast Red AL Salt and 0.1 M TBABF₄. Scan rate: 100 mV s^{-1} .

The rotating Pt ring-GC disk electrode (RRDE, 5 mm diameter) was polished to a mirror with 1.0 and $0.3 \mu\text{m}$ alumina slurries and subsequently sonicated in 1:1 HNO_3 , 1:1 ethanol and pure water for 3 min successively. Then, $4 \mu\text{L}$ 0.1 mg mL^{-1} GO suspension was sprayed onto the GC disk surface and allowed to dry at room temperature. This electrode was denoted as GO/GC. The ER-GO/GC electrode was prepared by potentiostatic reduction of GO/GC in N_2 -saturated 0.1 M phosphate buffered solution (PBS) at -1.0 V for 1.5 h. The AQ/ER-GO/GC electrode was prepared by electrochemical potentiodynamic reduction of 10 mM diazoniumsalt Fast Red AL Salt (Aldrich) in a 0.1 M tetrabutylammonium tetrafluoroborate (TBABF₄, Fluka) solution in acetonitrile with ER-GO/GC as working electrode, according to Tammeveski's method [8]. Potentiodynamic reduction was carried out by cycling the potential five times between 0.65 and -0.45 V at 100 mV s^{-1} . For comparison, the AQ/GC electrode was also synthesized by the same way. All the electrochemical

measurements were carried out with CHI 730D electrochemical analyzer combined with an EG&G PARC Model 636 electrode rotator system and an EG&G PARC frequency response detector (FRD 100). A Pt foil served as the counter electrode and a saturated calomel electrode (SCE) was used as a reference. The oxidation potential of Pt-ring electrode was set at +1.0 V vs SCE. The theoretical collection efficiency (N) calculated from the ratio of ring and disk currents of ferrocyanide/ferricyanide solution at the diffusion limiting conditions was 0.28, which agrees very closely with the N value determined from ring and disk geometry.

The images of scanning electron microscope (SEM) and transmission electron microscope (TEM) were obtained on FEI Quanta 200 FEG and JEM-2000 EX equipment, respectively. X-ray diffraction (XRD) measurements were carried out on a Japan Rigaku D/max-2400 ($\lambda = 1.54056 \text{ \AA}$) and operating at 40 kV and 200 mA. The pattern was taken at position-sensitive detector using a step size of 0.02° . Diffraction pattern was manually analyzed and identified in comparison with PCPDFWIN (2002) XRD analysis software. The Raman spectra were obtained by a Renishaw inVia M2000 spectrometer (UK) operating at He-Ne laser excitation (wavelength 633.8 nm, laser power 35 mW) with a beam spot size of about $2 \text{ }\mu\text{m}$. X-ray photoelectron spectroscopy (XPS) measurement was performed on an ESCALAB-MKII spectrometer (UK) with Al $K\alpha$ radiation (1486.6 eV) as the X-ray source for excitation. The XPS spectra were fitted using XPS peak 4.1 software in which a Shirley background was assumed.

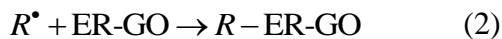
3. RESULTS AND DISCUSSION

3.1. Synthesis of ER-GO and AQ/ER-GO nanocomposite

After the GO suspension was uniformly sprayed onto the GC disk electrode surface, the potentiostatic reduction process was then applied to obtain the ER-GO/GC. It is obvious from Fig. 1 that there is a typical electrochemical irreversible reaction with a large current, which first increases and then decreases with the time, demonstrating the GO has been successfully reduced into ER-GO. The reduction of GO can also be identified from the color of ER-GO/ITO glass electrode, which changed from yellow-brown to black. The electrochemical reduction process exhibits three stages as previously reported [12] and can be interpreted as following. In the first stage, only GO which contacted directly with GC electrode, can be electrochemically reduced due to the dielectric GO. With the electrochemical reduction proceeding, more and more insulating GO turns to conducting ER-GO resulting in the obvious increase in reduction current. With the decrease of the amount of GO on GC electrode, the reduction current decays exponentially and finally reaches a stable value close to the background level at about 1500 s.

It is well known that a better method for the modification of carbon electrodes with quinones is covalently binding through the electrochemical reduction of appropriate diazonium salts of quinines [6,8,10]. In this work, grafting of AQ on ER-GO/GC surface was carried out by potentiodynamic electro-reduction of the corresponding diazonium salt, Fast Red A1 Salt, according to reaction (1) and (2):





As shown in Fig. 1(b), the grafting behaviour of the ER-GO/GC electrode with AQ followed the same trend as previously observed [6,8,9,31]. The first sweep shows a broad and irreversible cathodic peak at about 0.3 V, while at the subsequent fifth scan this peak is absent and shows only a negligible reduction current indicating the surface coverage of ER-GO/GC with grafted AQ.

3.2. Characterization of the synthesized materials.

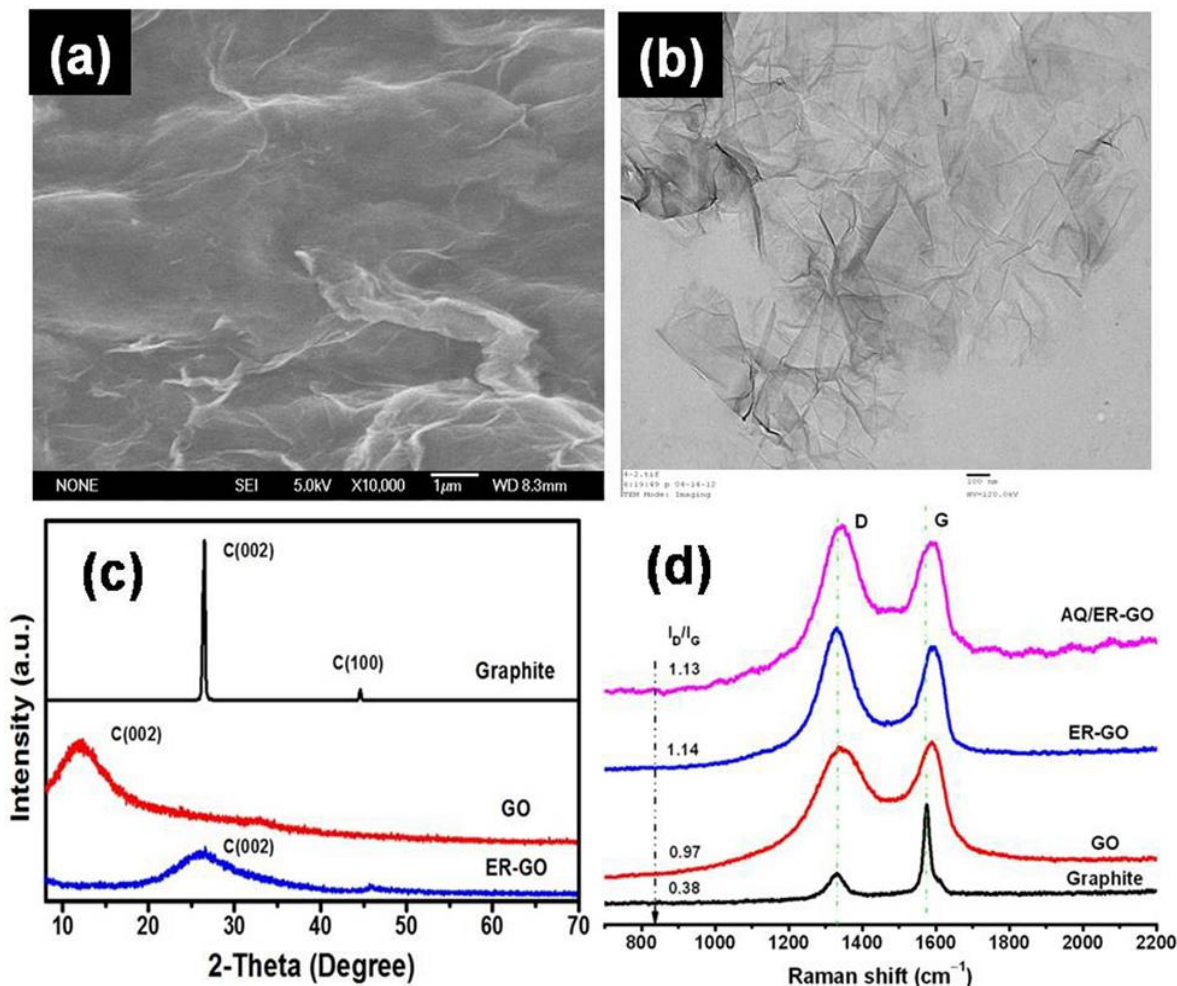


Figure 2. (a) and (b) SEM and TEM images of ER-GO samples, respectively; (c) XRD patterns of graphite, GO, ER-GO and (d) Raman spectra of graphite, GO, ER-GO and AQ/ER-GO.

Fig. 2(a) and (b) shows the SEM and TEM images of ER-GO nanosheets. The SEM image clearly indicates the folded and layered structures, which afforded ultrathin and homogeneous graphene films with kinked and wrinkled areas. The observed wrinkles is probably caused by the oxygen functionalization and the resultant defects during the preparation of GO [22]. Microstructure image in TEM revealed that the transparency ER-GO material consists of randomly oriented and

aggregated thin sheets with a wrinkled morphology over the entire substrate. Crumpling and scrolling are part of the intrinsic nature of graphene nanosheets, due to the 2D film structure [15,21,32].

Fig. 2(c) shows the XRD patterns of graphite, GO and ER-GO materials. It can be observed that after oxidation, the sharp diffraction peak of graphite ($2\theta = 26.2^\circ$, corresponding to the interlayer distance $d = 0.34$ nm and the (002) stacking of graphitic carbon [17,25,33]) disappeared, and a new feature diffraction peak ($2\theta = 11.3^\circ$) of GO appeared, corresponding to d-spacing of 0.85 nm, which is larger than that of graphite due to the intercalated oxygen functionalities and water molecules bonded on both sides of the graphene sheets [17]. After the electrochemical reduction, the XRD pattern shows the disappearance of the 11.3° peak and the reappearance of the (002) diffraction peak, which gives evidence the removal of some oxygen-containing functional groups and that the GO was reduced to graphene [14].

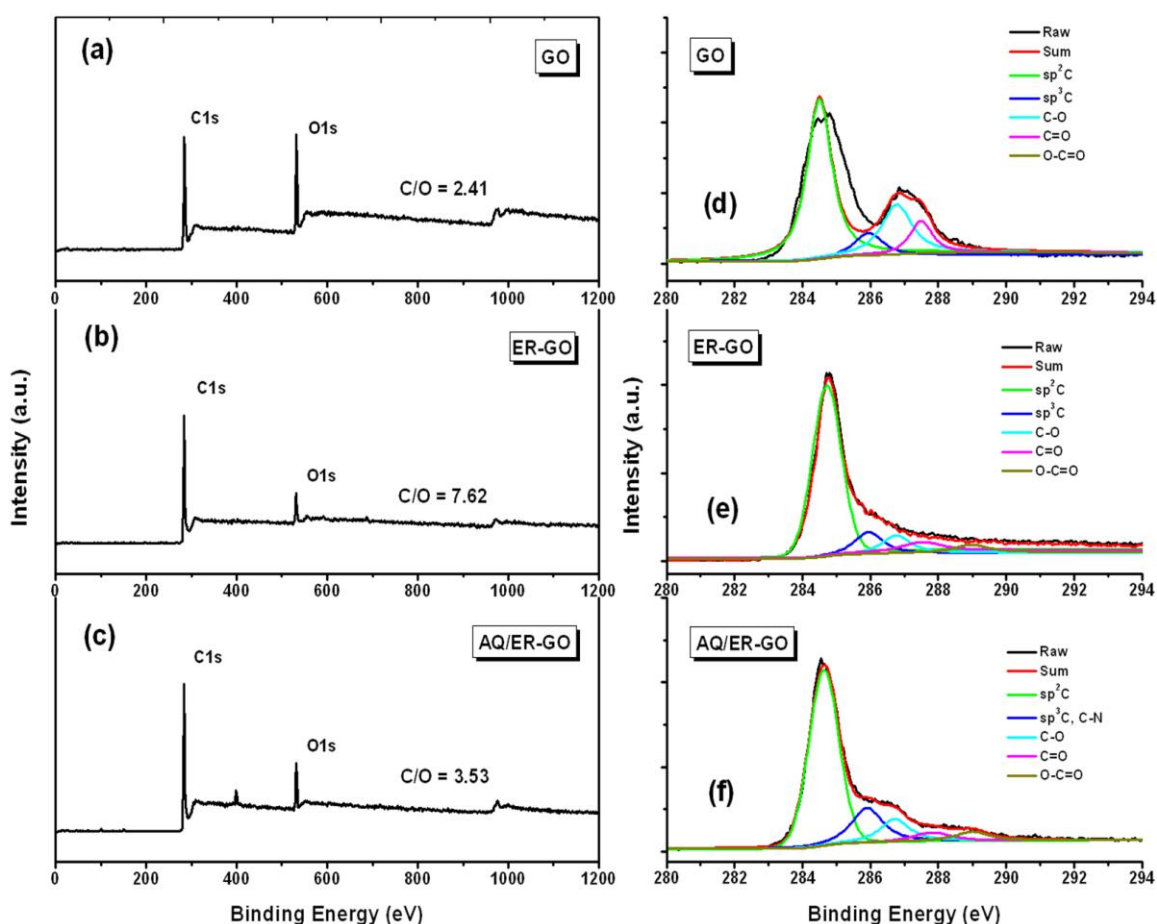


Figure 3. (a)-(c) XPS general spectra of GO, ER/GO, and AQ/ER-GO, respectively, (d)-(f) the corresponding curve fit of C1s spectra of (a)-(c).

Fig. 2(d) shows the Raman spectra of graphite, GO, ER-GO and AQ/ER-GO samples. The graphite displayed a prominent G band at 1584 cm^{-1} and a weak D band at 1340 cm^{-1} . For GO, the G band is broadened and shifted upward to 1596 cm^{-1} , and the D band increased substantially. The Raman spectra of ER-GO and AQ/ER-GO also contained both G and D bands at 1596 and 1340 cm^{-1} ,

respectively, with increased I_D/I_G intensity ratio compared to that in GO. It is well known that the intensity ratio of I_D/I_G provides the indication of the amount of structural defects and a quantitative measure of edge plane exposure [12,14,16]. The increased I_D/I_G ratio suggests a decrease in the average size of the in-plane sp^2 domains upon the electroreduction of GO and significant number of defects in ER-GO and AQ/ER-GO.

The reduction degree of GO and the chemical compositions of ER-GO and AQ/ER-GO were also characterized by XPS. The wide scan XPS spectra of GO and RGO shown in Fig. 3(a)-(c) display the presence of only carbon and oxygen atoms for GO and ER-GO materials, while a new peak at approximate 402 eV corresponding to N 1s [17,20,25] appeared for AQ/ER-GO sample, which may be attributed to the incomplete electroreduced AQ diazonium salt on ER-GO surface. Additionally, the reduction degree of GO can be measured by the ratio of C1s to O1s peak areas (C/O) in XPS spectrum. The C/O atomic ratio of ER-GO and AQ/ER-GO increases clearly after the electro-reduction of GO, indicating the successful deoxygenation of GO. The core level high resolution C 1s XPS spectra for GO, ER-GO and AQ/ER-GO are shown in Fig. 3(d)-(f). From the C 1s XPS spectrum of GO, five different peaks centered at 284.5, 285.6, 286.8, 287.5, and 289.2 eV were observed, which are assigned to sp^2 C, sp^3 C, C–O (hydroxyl and epoxy), C=O (carbonyl) and O–C=O (carboxyl) oxygen-containing functional groups, respectively. These results agree well with those of previous studies [16,25,26]. After the electro-reduction of GO, the spectrum of ER-GO shows that the intensities of C 1s peaks of the carbons binding to oxygen and the peak of sp^3 C decrease, while the peak of sp^2 C increases accordingly, revealing that most of the oxygen-containing functional groups are removed and the efficient reduction of GO. For the C 1s XPS spectrum of AQ/ER-GO, it is too difficult to distinguish the sp^3 C and C–N bond peaks, because they are mixed together at the binding energy of 285.6 eV. But it is seen from the enhanced shoulder in the binding energy range of 285.0–290.0 eV in C1s spectra that carbon structure defects are produced on ER-GO after AQ grafting.

3.3. CV studies on the electrocatalytic ORR.

To investigate the electrochemical behaviors and electrocatalytic activities towards ORR of the bare and different modified GC electrodes, CVs were measured in N_2 - and O_2 -saturated 0.1 M KOH solutions between 0.10 V and –1.50 V. As can be observed from Fig. 4:

(I) In N_2 -saturated solution, the CV behavior of the bare GC presents no obvious cathodic peak except that a small amount of hydrogen evolves at potentials more negative than –1.3 V. While a pair of weak reversible redox peaks at ca. –0.40 V was obtained at ER-GO/GC electrode, which can be ascribed to the residual quinone-like groups on ER-GO nanosheets surface. Furthermore, a pair of apparent redox peak for the surface confined quinones, corresponding to the AQ/AQH₂ couple [10] was observed for AQ and AQ/ER-GO functionalized GC electrodes. The redox potential of the covalently attached AQ was ca. –0.85 V vs SCE, in agreement with previous results obtained in the same solution [6–8,10]. In comparison to the bare GC and AQ/GC, the ER-GO and AQ/ER-GO functionalized GC electrodes exhibit larger background currents.

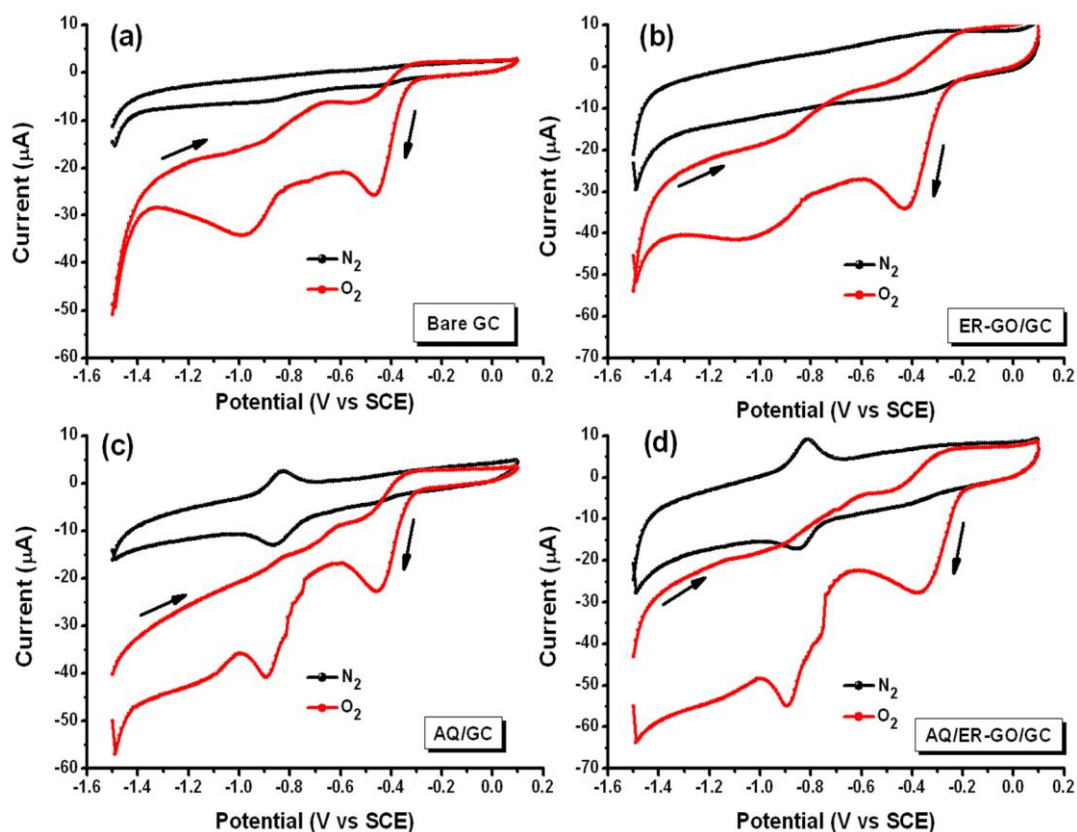
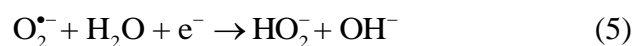
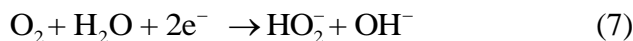


Figure 4. Cyclic voltammograms of (a) bare GC, (b) ER-GO/GC, (c) AQ/GC, and (d) AQ/ER-GO/GC electrodes in N_2 - and O_2 -saturated 0.1 M KOH. Scan rate: 20 mV s^{-1} .

(II) In O_2 -saturated solution, two well-defined oxygen reduction peaks were observed on all the studied electrodes in the potential window employed. Additionally, there are no apparent oxidation peaks in the course of anodic scan demonstrating that the ORR on these electrodes is irreversible. All the two reduction peaks are separated completely implying two steps of oxygen reduction.

(i) For the bare GC and ER-GO/GC electrodes, the first reduction peak located at ca. -0.45 and -0.4 V, respectively, can be attributed to the $2e^-$ electrochemical reduction of O_2 mediated by the active surface quinone-like groups with superoxide anion ($O_2^{\bullet-}$) as the intermediate (reactions (3)–(6)) [14,27,34], while in the more negative potentials range from ca. -0.6 to -1.2 V, broad reduction peaks can be observed which may be due to the two unseparate reduction processes. In other words, at the second step of both the bare GC and ER-GO/GC, O_2 is firstly transformed into HO_2^- by a direct $2e^-$ reduction (reaction (7)) on the native GC and ER-GO/GC surface, respectively, and subsequently partial HO_2^- is reduced to OH^- (reaction (8)).





(ii) For the ER-GO and AQ/ER-GO modified GC electrodes, the first reduction process is similar to that occurred on the GC and ER-GO/GC electrodes, and more importantly, the second reduction peak centered at ca. -0.87 V was apparently observed, which is electrochemically mediated by the grafted AQ on GC and ER-GO/GC surfaces. Additionally, a weak unobvious reduction peak at ca. -1.1 V was also observed on both electrodes, which corresponds to the further reduction of HO_2^- to produce OH^- (reaction (8)). After the functionalization with ER-GO, the onset potential of ORR for the AQ/ER-GO electrode shifted positively with a more increased current of the two cathodic peaks in comparison to the bare GC and AQ/GC electrodes. This result clearly indicates that the modification of GC with ER-GO nanosheets plays a key role for ORR activity enhancement of grafted AQ.

3.4. RDE studies on the electrocatalytic ORR.

To obtain insight into the electron transfer kinetics of the ORR, we studied the reaction kinetics in O_2 -saturated 0.1 M KOH by rotating disk voltammetry from 200 to 1000 rpm. In general, high scan rate results in large peak current. In this work, scan rate of 10 mV s^{-1} is very low and the electrode reaction is close to steady state process, which is beneficial to RDE and RRDE researches. The voltammetric profiles in Fig. 5(a1)-(d1) show that the current is enhanced with the increase in the rotation rate, due to the faster oxygen flux to disk electrode surface at higher rotation speeds.

(I) For the bare GC and ER-GO/GC electrodes, a series of prewaves mediated by surface quinone-like groups which present on the native GC and ER-GO surface and act as the electron transfer mediator, were also observed. Numerous active native quinone-like groups on the polished GC surface results in the current maximum at ca. -0.5 V, while the current minimum at ca. -0.7 V is due mainly to the decrease in the number of electrocatalytic active surface sites for oxygen reduction [6–8]. At more negative potential, the GC surface itself appears to be active enough to catalyse ORR and the disk current increases accordingly. Different from the bare GC and the result obtained in CV, three reduction steps are recorded at ER-GO/GC electrode. In addition, ER-GO functionalization results in an obvious positive shift of the ORR onset potential.

(II) For AQ and AQ/ER-GO functionalized GC electrodes, the ORR prewaves which correspond to that observed for the bare GC and ER-GO electrodes were also obtained. This phenomenon accords with the fact that in spite of surface functionalized by anthraquinone, the very active quinone-like groups of native GC responsible for the first reduction wave are still present [8]. Compared to the bare GC and ER-GO electrodes, the prewave current is lower indicating that the attached AQ partially blocks the native GC and ER-GO surface sites, therefore decrease the rate of

ORR. Additionally, no current minimum value was observed on the two sets of polarization curves in the prewave range.

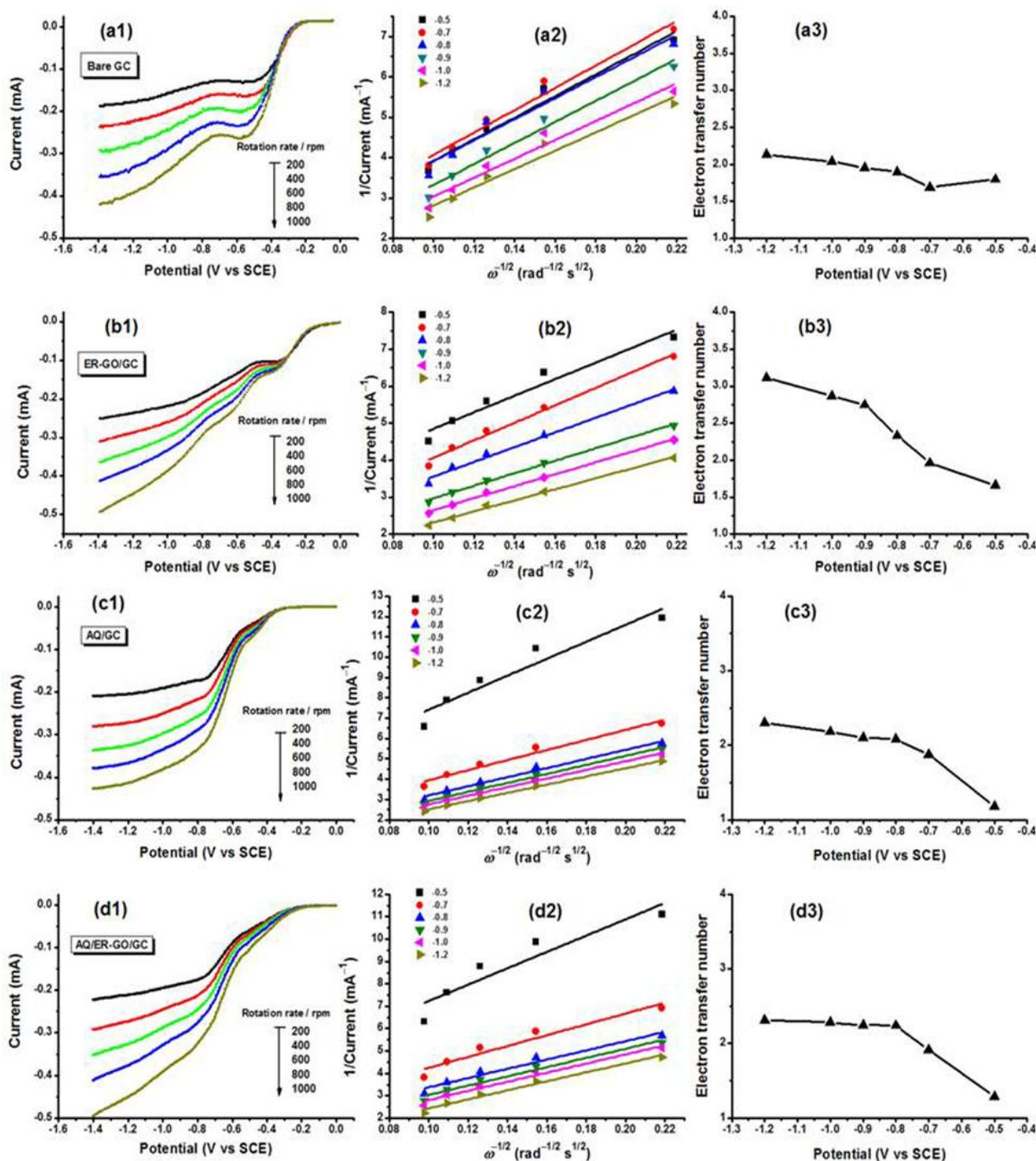


Figure 5. (a1)-(d1) RDE voltammetry curves for ORR on bare GC, ER-GO/GC, AQ/GC, and AQ/ER-GO/GC electrodes in O₂-saturated 0.1 M KOH at different rotation rates. Scan rate: 10 mV s⁻¹, (a2)-(d2) and (a3)-(d3) the corresponding Koutecky–Levich plots and the dependence of transferred electron number, *n*, on potential of (a1)-(d1), respectively.

The second O₂ reduction wave starts at about -0.6 V in both cases, which is more positive compared to the redox potential of the AQ/GC and AQ/ER-GO/GC electrodes (Fig. 4(c) and (d)), indicating the strong electrocatalytic effect of the grafted AQ on ORR. It is proposed by Tammeveski [8,10] that this is due to the high chemical reactivity of the intermediate semiquinone with O₂ (reactions (3) and (4)) at potentials much more positive than the formal potential of surface attached AQ.

The corresponding Koutecky–Levich plots (I^{-1} vs $\omega^{-1/2}$) at various electrode potentials show good linearity (Fig. 5(a2)-(d2)). Linearity and parallelism of the plots are considered as typical of first-order reaction kinetics with respect to the concentration of dissolved O₂. The kinetic parameters can be analyzed on the basis of the Koutecky–Levich equations [35]:

$$\frac{1}{I} = \frac{1}{I_L} + \frac{1}{I_k} = -\frac{1}{B\omega^{1/2}} - \frac{1}{I_k} \quad (9)$$

$$B = 0.62nFAD_{O_2}^{2/3}\gamma^{-1/6}c_{O_2} \quad (10)$$

$$I_k = nFAkc_{O_2} \quad (11)$$

in which I is the measured current, I_k and I_L are the kinetic and diffusion-limiting currents, ω is the angular velocity of the disk, n is the overall number of electrons transferred in ORR, F is the Faraday constant (96,485 C mol⁻¹), c_{O_2} is the bulk concentration of O₂, ν is the kinematic viscosity of the electrolyte, and k is the electron transfer rate constant. As shown in Fig. 5(a3)-(d3), the number of electrons transferred (n) can be obtained from the slope of the Koutecky–Levich plots by using parameters: $c_{O_2} = 1.2 \times 10^{-3}$ M, $D_{O_2} = 1.9 \times 10^{-5}$ cm s⁻¹, and $\nu = 0.01$ cm² s⁻¹ in 0.1 M KOH [8].

(I) For the bare GC electrode, the deduced value of n is close to two at the potentials of the prewave and increases slightly ($n = 1.8$ – 2.13), which indicates that a small fraction of HO₂⁻ produced can be further reduced at more negative potentials. But the variation of n with potential on the ER-GO/GC electrode is quite different. The values of n are between 1.55 and 3.11. The increase in n at more negative potentials is probably due to that HO₂⁻ produced can be further reduced via the catalysis of ER-GO nanosheets, which is governed by a higher over-potential. The result is in good agreement with the previous report that C-graphene nanosheets possess excellent catalytic activity in facilitating the 4e⁻ ORR through a two-step, two-electron process [14,17,26,27].

(II) For the ER-GO and AQ/ER-GO modified electrodes, the variation of n with potential follows the similar trend that the electron transfer number increased slightly with a decrease in the negative potential. In addition, it is worth noting that the values of n at prewave potential are far lower than 2.0 and also less than that determined on the bare GC and ER-GO/GC electrodes. This observation provides the evidence that the intermediate O₂^{•-} electrogenerated in prewave range with no proton involvement could diffuse to homogeneous solution [3,8], due to the partial blocking of the surface adsorption sites by grafted AQ.

3.5. RRDE studies on the electrocatalytic ORR.

To further verify the ORR selectivity and pathway on bare GC, AQ/GC, ER-GO/GC and AQ/ER-GO/GC electrodes, the formation of HO_2^- during the ORR process was monitored using RRDE measurement at rotation rate of 800 rpm, as shown in Fig. 6.

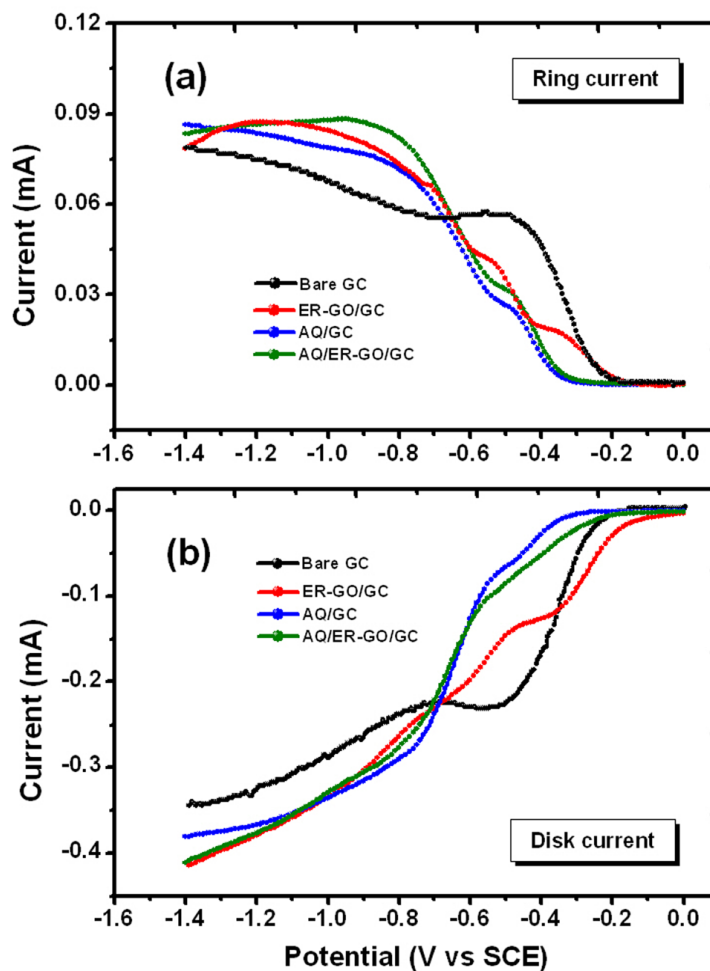


Figure 6. RRDE current-potential curves of bare GC, ER-GO/GC, AQ/GC, and AQ/ER-GO/GC disk (a)-Pt ring (b) electrodes recorded in O_2 -saturated 0.1 M KOH with a rotation rate of 800 rpm. Scan rate: 10 mV s^{-1} .

Similar to the results of CVs, ring current of the bare GC, AQ/GC and AQ/ER-GO/GC electrodes exhibits two oxidation peaks, and three oxidation steps was similarly observed on the ring current of ER-GO/GC electrode, suggesting our reasonable definition of the reduction peaks in CVs. The AQ/ER-GO/GC electrode leads to ca. 100 mV positive shift of the ORR onset potential compared to AQ/GC electrodes.

The electron transfer number (n) and the % HO_2^- can be determined by the followed equations [6] and the results are shown in Fig. 7(a) and (b), respectively.

$$n = \frac{4NI_D}{(NI_D + I_R)} \tag{12}$$

$$\%HO_2^- = \frac{200I_R}{(NI_D + I_R)} \tag{13}$$

where I_D is disk current, I_R is ring current and N is current collection efficiency of the Pt ring.

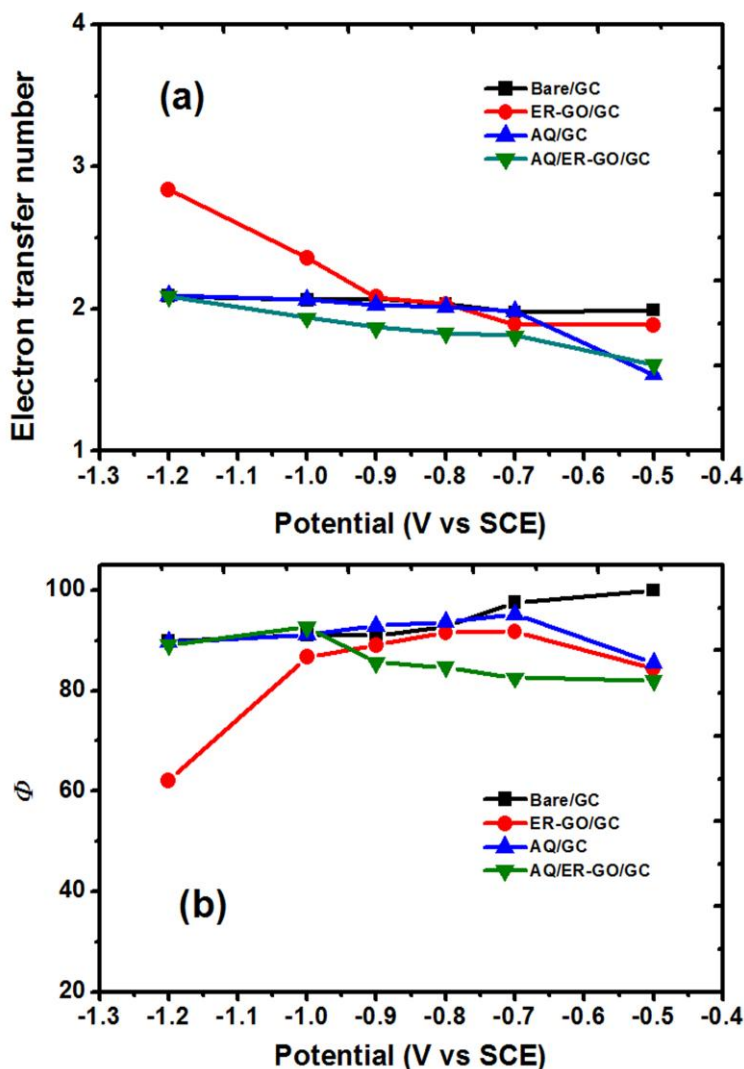


Figure 7. The dependence of n (a) and $\%HO_2^-$ (b) on potential calculated from the RRDE data in Figure 6.

From the RRDE data, the values of n at more negative disk potentials is not 2 but larger than 2, which is consistent with the data obtained from the slopes of Koutecky–Levich plots. This observation also provides the evidence that the processes of ORR at these electrodes may possibly include several parallel processes. One is the production of HO_2^- and the second is further reduction of HO_2^- to give

OH^- involving its disproportionation (reaction (14)) to O_2 that could be reduced again via the $2e^-$ pathway, which results in the ring currents not consistent decrease with the negatively shifting of potential.



Furthermore, very different case is that the third reduction process on the ER-GO/GC disk electrode is attributed to the effective reduction of HO_2^- catalyzed by ER-GO nanosheets at more negative potentials, and at the same time O_2 generated from the disproportionation reaction may be reduced via a coexisting $2e^-$ and $4e^-$ pathway, which is supported by the decrease in ring current, the increase in n value and the decrease in HO_2^- productivity. These results indicate that the HO_2^- pathway is preferentially followed on the AQ functionalized ER-GO modified electrodes, corroborating the AQ/ER-GO nanocomposite is a promising metal-free catalyst for the ORR in alkaline medium.

4. CONCLUSIONS

In this paper, AQ functionalized ER-GO nanocomposites have successfully synthesized by a facile electrochemical potentiostatic-potentiodynamic method using GO and Fast Red A1 salt as the starting materials. The ER-GO and AQ/ER-GO nanocomposites as advanced electrode materials were extensively investigated by various characterization methods, including SEM, TEM, XRD, Raman, and XPS. It has been demonstrated that the electrochemical reduction method is a simple, low-cost, efficient and environmentally friendly strategy to fabricate ER-GO films with high C/O ratio. After successful grafting of AQ onto the ER-GO nanosheets surface, the resulting AQ/ER-GO nanocomposite modified electrode exhibits an enhanced catalytic activity towards ORR in alkaline medium as an efficient metal-free electrocatalyst, which outperforms sole ER-GO and AQ modified GC electrodes in ORR current density at medium overpotentials. At AQ/ER-GO/GC electrode dissolved oxygen undergoes two successive $2e^-$ reduction processes with HO_2^- as intermediate, and at more negative potentials the ER-GO nanosheets can efficiently catalyzes the further reduction of partial HO_2^- to produce OH^- .

ACKNOWLEDGMENT

This work was financially supported by the National Natural Science Foundation of China (No.21177017) and the Fundamental Research Funds for the Central Universities [No.DUT10RC(3)113].

References

1. Y. Kiros, *Int. J. Electrochem. Sci.*, 2 (2007) 285
2. D. Morales-Acosta, D. López de la Fuente, L.G. Arriaga, G.V. Gutiérrez and F.J. Rodríguez Varela, *Int. J. Electrochem. Sci.*, 6 (2011) 1835
3. E. Brillas, I. Sirés, and M.A. Oturan, *Chem. Rev.*, 109 (2009) 6570
4. H.H. Yang and R.L. McCreery, *J. Electrochem. Soc.*, 147 (2000) 3420
5. B. Šljukić, C.E. Banks, and R.G. Compton, *J. Iran. Chem. Soc.*, 2 (2005) 1

6. F.Mirkhalaf, K.Tammeveski and D.J. Schiffrin, *Phys. Chem. Chem. Phys.*, 6 (2004) 1321
7. G. Jürmann, D.J. Schiffrin, and K. Tammeveski, *Electrochim. Acta*, 53 (2007) 390
8. K. Tammeveski, K. Kontturi, R.J. Nichols, R.J. Potter, and D.J. Schiffrin, *J. Electroanal. Chem.*, 515 (2001) 101
9. K. Vaik, A. Sarapuu, K. Tammeveski, F. Mirkhalaf, and D.J. Schiffrin, *J. Electroanal. Chem.*, 564 (2004) 159
10. A. Sarapuu, K. Vaik, D.J. Schiffrin, and K. Tammeveski, *J. Electroanal. Chem.*, 23 (2003) 541
11. A. Salimi, M.F. Mousavi, H. Eshghi, H. Sharghi, and M. Shampsipur, *Bull. Chem. Soc. Jpn.*, 72 (1999) 2121
12. M. Zhou, Y.L. Wang, Y.M. Zhai, J.F. Zhai, W. Ren, F.A. Wang, and S.J. Dong, *Chem. Eur. J.*, 15 (2009) 6116
13. D. Chen, L.H. Tang, and J.H. Li, *Chem. Soc. Rev.*, 39 (2010) 3157
14. L.H. Tang, Y. Wang, Y.M. Li, H.B. Feng, J. Lu, and J.H. Li, *Adv. Funct. Mater.*, 19 (2009) 2782
15. D. S.Geng, Y.Chen, Y. G. Chen, Y.L. Li, R. Y. Li, X. L. Sun, S. Y. Ye, and S. Knights, *Energy Environ. Sci.*, 4 (2011) 760
16. Z. J. Fan, W. Kai, J. Yan, T. Wei, L. J. Zhi, J. Feng, Y. M. Ren, L. P. Song, and F. Wei, *ACS Nano*, 5 (2011) 191
17. L.T. Qu, Y. Liu, J.B. Baek, and L.M. Dai, *ACS Nano*, 4 (2010) 1321
18. A.A. Elzatahry, A.M. Abdullah, T.A.S. El-Din, A.M. Al-Enizi, A.A. Maarouf, A. Galal, H.K. Hassan, E.H. El-Ads, S.S. Al-Theyab and A.A Al-Ghamdi, *Int. J. Electrochem. Sci.*, 7 (2012) 3115
19. J.J. Wu, D. Zhang, Y. Wang, Y. Wan, and B.R. Hou, *J. Power Source*, 198 (2012) 122
20. M. Jahan, Q.L. Bao, and K.P. Loh, *J. Am. Chem. Soc.*, 134 (2012) 6707
21. Y.Y. Shao, S. Zhang, M.H. Engelhard, G.S. Li, G.C. Shao, Y. Wang, J. Liu, I.A. Aksay, and Y.H. Lin, *J. Mater. Chem.*, 20 (2010) 7491
22. X.M. Feng, R.M. Li, Y.W. Ma, R.F. Chen, N.E. Shi, Q.L. Fan, and W. Huang, *Adv. Funct. Mater.*, 21 (2011) 2989
23. H. J. Salavagione, G. Martínez, and G. Ellis, *Macromol. Rapid Commun.*, 32 (2011) 1771
24. Z. Yang, Z. Yao, G.F. Li, G.Y. Fang, H.G. Nie, Z. Liu, X.M. Zhou, X.A. Chen, and S.M. Huang, *ACS Nano*, 6 (2012) 205
25. H.R. Byon, J. Suntivich, and S.H. Yang, *Chem. Mater.*, 23 (2011) 3421
26. K.R. Lee, K.U. Lee, J.W. Lee, B.T. Ahn, S.I. Woo, *Electrochem. Commun.*, 12 (2010) 1052
27. J.J. Wu, Y. Wang, D. Zhang, and B.R. Hou, *J. Power Source*, 196 (2011) 1141
28. Y.F. Zhou, G.Q. Zhang, J. Chen, G.E. Yuan, L. Xu, L.F. Liu, and F.L. Yang, *Electrochem. Commun.*, 22 (2012) 69
29. T. Nagaoka, T. Sakai, K. Ogura, and T. Yoshino, *Anal. Chem.*, 58 (1986) 1953
30. W.S. Hummers, and R.E. Offeman, *J. Am. Chem. Soc.*, 80 (1958) 1339
31. P. Allongue, M. Delamar, B. Desbat, O. Fagebaume, R. Hitmi, J. Pinson, and J.M. Savéant, *J. Am. Chem. Soc.*, 119 (1997) 201
32. J.C. Meyer, A.K. Geim, M.I. Katsnelson, K.S. Novoselov, T.J. Booth, and S. Roth, *Nature*, 446 (2007) 60
33. F.Y. Zhang, Z.H. Wang, Y.Z. Zhang, Z.X. Zheng, C.M. Wang, Y.L. Du, and W.C. Ye, *Int. J. Electrochem. Sci.*, 7 (2012) 1968
34. Z.W. Zhang, D. Tyrk, and E. Yeager, in *Proceedings of the Workshop on the Electrochemistry of Carbon*, S.A. Sarangapani, J. R. Akridge, and B. Schumm, Editors, p. 158, The Electrochemical Society, Pennington, NJ (1984)
35. A.J. Bard and L.R. Faulkner, *Electrochemical Methods: Fundamentals and Applications*, second ed., John Wiley & Sons Inc., New York (2001)